Transition path sampling and Supersymmetricmoleculardynamics

Slides by Russell Hanson
June 27, ‘07

Part I – Transition path sampling: Throwing Ropes Over Rough Mountain Passes, in the Dark

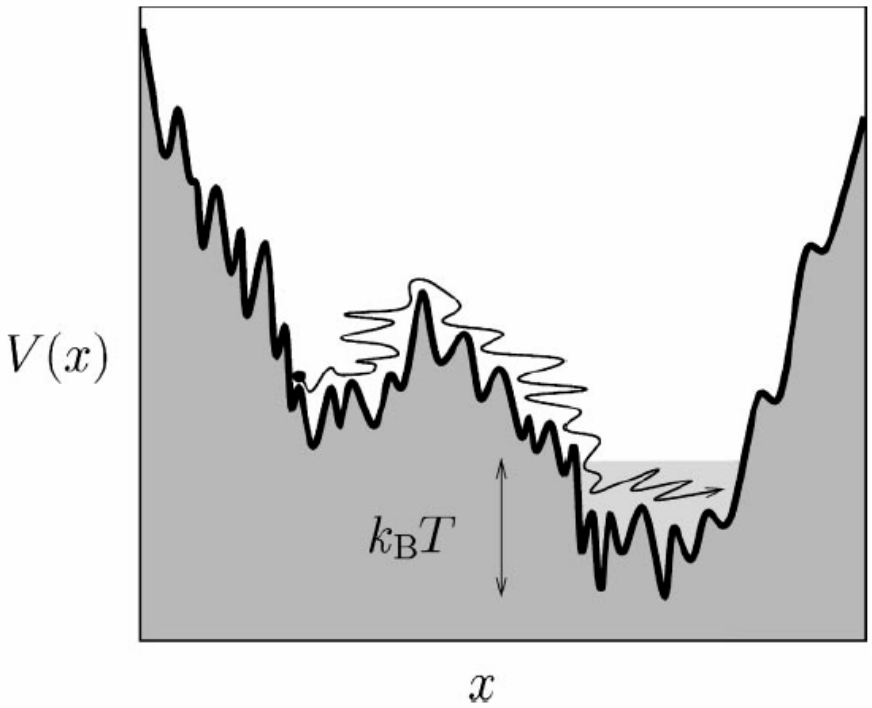

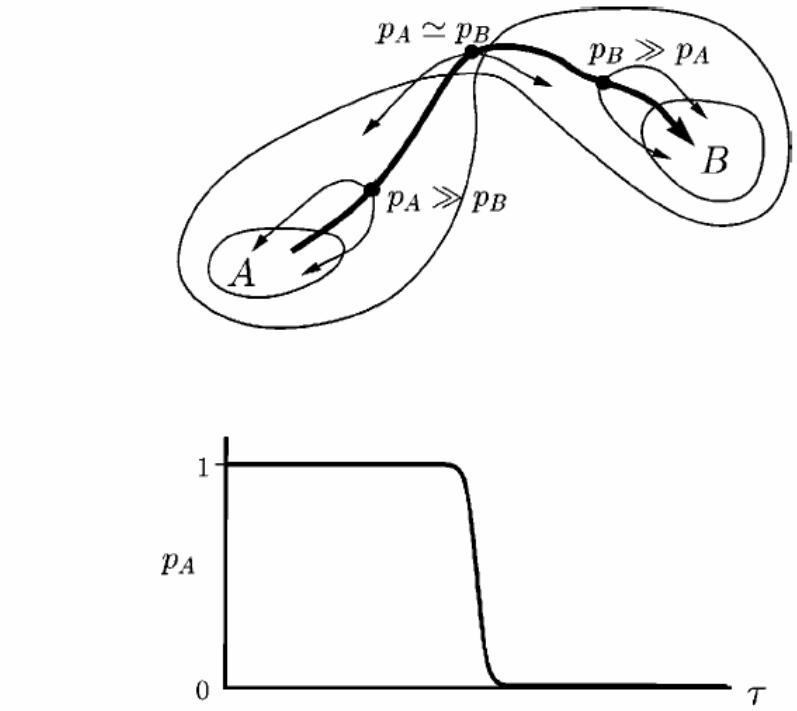

Figure 7 The committor, p_A, is computed along a single path in the transition path ensemble (thick solid line, top panel) by determining the percentage of fleeting trial trajectories starting from the configuration at time slice τ (with random momenta) that has reached region A in a time t. Typically 10–100 of these fleeting trajectories are needed to obtain p_A accurately. For instance, $p_A \approx 1$ for the left time slice in the top panel, because nearly all trajectories started from that time slice end in A. The configurations for which $p_A \simeq p_B$ are considered transition states.

Annu. Rev. Phys. Chem. 2002. 53:291–318

Population operators

$h_A(x)$

$h_B(x)$

x is a point in phase space (configuration space and momentum space)

When x is within region A

$$h_A(x) = 1$$

otherwise

$$h_A(x) = 0$$

For trajectory of time duration t

$$x(t) = (x_0, x_1, \ldots, x_t)$$

Statistical weight for the rare trajectories connecting A and B is

$$h_A(x_0)\, \rho[x(t)]\, h_B(x_t)$$

$\rho[x(t)]$ is unconstrained distribution functional for trajectories.

For deterministic trajectories:

$$\rho[x(t)] = \rho(x_0) \prod_{\text{all } t' \le t} \delta[x_{t'} - x_{t'}(x_0)]$$

↳ unconstrained dist'n of initial phase space points, x_0.

Transition path sampling is importance sampling for the dist'n $h_A(x_0)\, \rho[x(t)]\, h_B(x_t)$

Acceptance probability for trial step is

$$\min\left[1, \frac{w(x, x', \delta)\, h_A(x_0')\, \rho(x_0')\, h_B(x_t')}{h_A(x_0)\, \rho(x_0)\, h_B(x_t)\, w(x', x, -\delta)}\right].$$

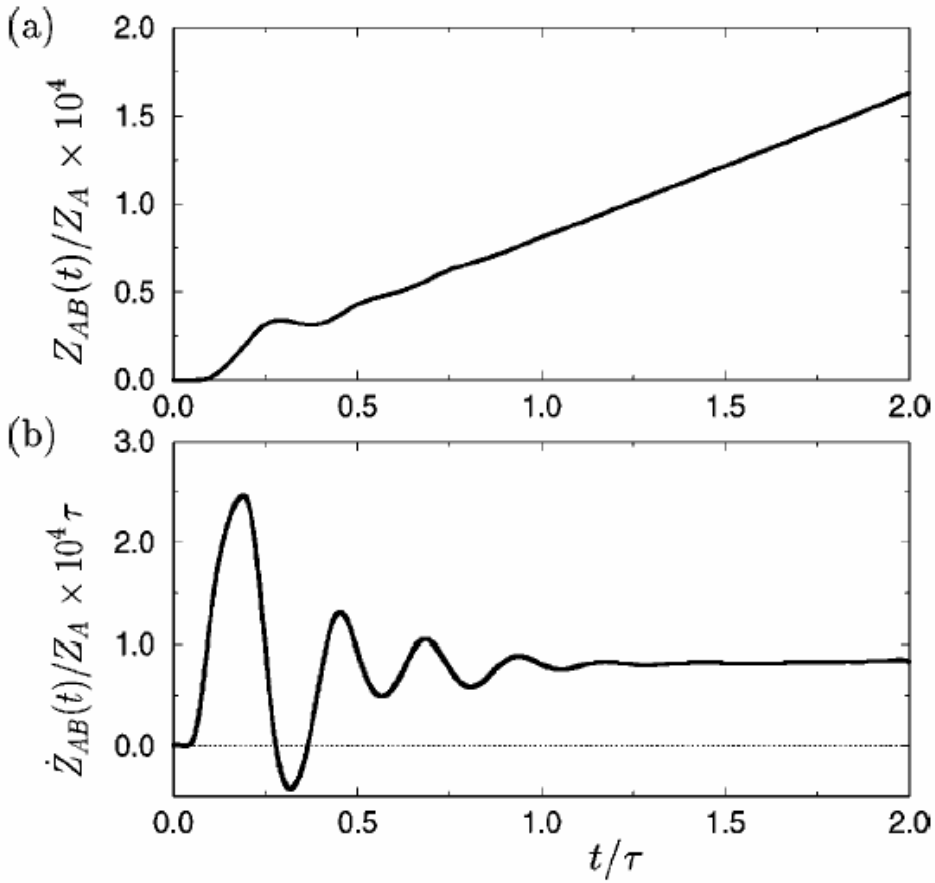

$$Z_{AB}(t) = \sum_{\chi(t)} \rho[\chi(t)]\, h_A(\chi_0)\, h_B(\chi_t).$$

$$\sum_{\chi(t)} \rho[\chi(t)]\, h_A(\chi_0) = \sum_{\chi_0} \rho(\chi_0) h_A(\chi_0) = Z_A,$$

Figure 5 (*a*) The ratio of partition functions $Z_{AB}(t)$ and Z_A as a function of time t, calculated using the scheme illustrated in Figure 4, for the process described in the section "Isomerization of a Solvated Model Dimer," below. For times longer than that required to commit to a basin of attraction ($\approx\tau$ in this example) but short compared to the characteristic time of spontaneous transitions, this ratio is a linear function of time. (See Equation 8.) The corresponding slope, i.e., the plateau value of $d[Z_{AB}(t)/Z_A]/dt$ in (*b*), is the rate constant for transitions from A to B.

2.1 Transition path sampling

The calculation of the transition rate using the transition path ensemble (TPE) technique consists of several steps (details of this technique can be found in ref. 4 and 5):

1. Define the function $h_R(x)=1$ when $x \in R$ and $h_R(x)=0$ otherwise, where R is either region A or B. This defines the two stable sites. The transition from A to B should be rare.

2. Compute the probability $\langle h_B(t) \rangle$ that a path of length T starting in A ends in B after a time t provided that it has been in B at least once during the time interval $[0,T]$:

$$\langle h_B(t) \rangle = \frac{\int dx_0 \exp[-\beta \mathcal{H}(x_0)] h_A(x_0) H_B(x_0, T) h_B(x_t)}{\int dx_0 \exp[-\beta \mathcal{H}(x_0)] h_A(x_0) H_B(x_0, T)} = \frac{\int dx_0 F(x_0, T) h_B(x_t)}{\int dx_0 F(x_0, T)} \quad (1)$$

in which $t \in [0,T]$ and

$$H_B(x_0, T) = \max_{0 \le t \le T} h_B(x_t) \quad (2)$$

$$F(x_0, T) = \exp[-\beta \mathcal{H}(x_0)] h_A(x_0) H_B(x_0, T) \quad (3)$$

Here, we have assumed the following:

(a) All paths are deterministic, *i.e.* the position of the end of the path (x_t) follows directly from the initial condition x_0 by integrating the equations of motion, *i.e.* $x_t = x_t(x_0)$. We will use

molecular dynamics (MD) in the microcanonical (NVE) ensemble for this.

(b) The initial conditions x_0 are taken from a Boltzmann distribution, *i.e.* the total energy of a path (which is constant along a path because the path itself is obtained by a MD simulation in the NVE ensemble) is sampled in the canonical ensemble.

3. Compute the probability $C(t)$ that a path that starts in A ends in B after time t. For this, we can write

$$C(t) = \frac{\int \mathrm{d}x_0 \exp[-\beta \mathscr{H}(x_0)] h_{\mathrm{A}}(x_0) h_{\mathrm{B}}(x_t)}{\int \mathrm{d}x_0 \exp[-\beta \mathscr{H}(x_0)] h_{\mathrm{A}}(x_0)} = \int_{\lambda_{\min}}^{\lambda_{\max}} \mathrm{d}\lambda P(\lambda, t) \quad (4)$$

in which

$$P(\lambda, t) = \frac{\int \mathrm{d}x_0 \exp[-\beta \mathscr{H}(x_0)] h_{\mathrm{A}}(x_0) \delta[\lambda - \lambda(x_t)]}{\int \mathrm{d}x_0 \exp[-\beta \mathscr{H}(x_0)] h_{\mathrm{A}}(x_0)} \quad (5)$$

Here, we have defined region B using an order parameter λ in such a way that region B is between $\lambda_{\min}$ and $\lambda_{\max}$. $P(\lambda,t)$ can be interpreted as the probability for the system to be in a state with a certain λ after time t given that the system is in A at time 0. Because $P(\lambda,t)$ is quite small in B (*i.e.* transitions from A to B are rare), it is advantageous to use umbrella sampling[14–16] to compute $P(\lambda,t)$. By defining overlapping regions B_i by

$$x_t \in \mathrm{B}_i \qquad \text{if} \qquad \lambda_{\min}(i) \leq \lambda(x_t) \leq \lambda_{\max}(i) \quad (6)$$

in such a way that the union of B_i equals the total phase space, one is able to calculate

$$P(\lambda, t, i) = \frac{\int \mathrm{d}x_0 \exp[-\beta \mathscr{H}(x_0)] h_{\mathrm{A}}(x_0) h_{\mathrm{B}_i}(x_t) \delta[\lambda - \lambda(x_t)]}{\int \mathrm{d}x_0 \exp[-\beta \mathscr{H}(x_0)] h_{\mathrm{A}}(x_0) h_{\mathrm{B}_i}(x_t)} = \frac{\int \mathrm{d}x_0 f(x_0, t, i) \delta[\lambda - \lambda(x_t)]}{\int \mathrm{d}x_0 f(x_0, t, i)} \quad (7)$$

in which

$$f(x_0, t, i) = \exp[-\beta \mathscr{H}(x_0)] h_{\mathrm{A}}(x_0) h_{\mathrm{B}_i}(x_t) \quad (8)$$

$f(x_0,t,i)$ is the ensemble of all paths starting in A and ending in B_i at time t. Because $P(\lambda,t,i) \propto P(\lambda,t,j)$, one is able to construct $P(\lambda,t)$ by matching the histograms and normalizing.

4. Finally, the transition rate $k_{\mathrm{A}\to\mathrm{B}}$(number of events per unit of time) is calculated using

$$k_{\mathrm{A}\to\mathrm{B}} = \frac{\mathrm{d}C(t)}{\mathrm{d}t} = \frac{C(t')}{\langle h_{\mathrm{B}}(t')\rangle_{F(x_0,T)}} \times \frac{\mathrm{d}\left[\langle h_{\mathrm{B}}(t)\rangle_{F(x_0,T)}\right]}{\mathrm{d}t} \qquad (9)$$

The quantities $\langle h_{\mathrm{B}}(t)\rangle$[eqn. (1)] and $P(\lambda,i)$[eqn. (7)] can be interpreted as ensemble averages over distributions $F(x_0,T)$ and $f(x_0,t,i)$, respectively. As these ensemble averages are averages over paths starting in A (represented by the initial condition x_0), the resulting ensemble is called the transition path ensemble. Therefore, one can use a conventional MC procedure to sample from these distributions. The trial moves for sampling from these distributions are described in detail in ref.5 and briefly mentioned in section 3.

Partial path sampling

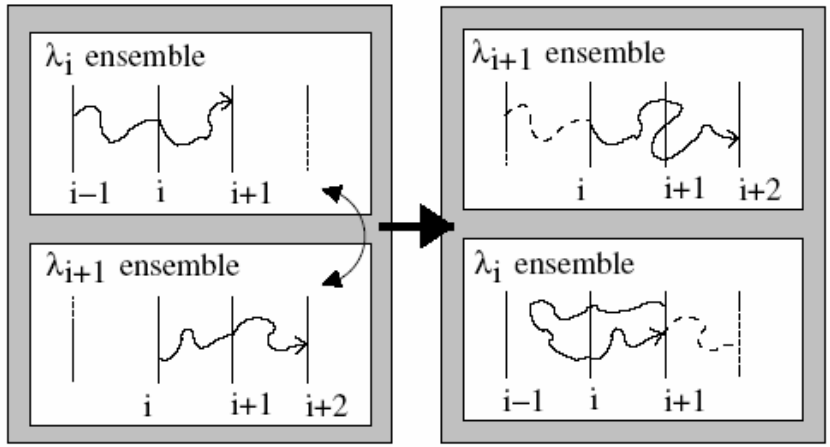

Fig. 3. Path swapping move for PPTIS. The last half of the path in the λ_i ensemble and the first half of the path in the λ_{i+1} are swapped to the λ_{i+1} and λ_i ensembles, respectively.

Time as transition parameter

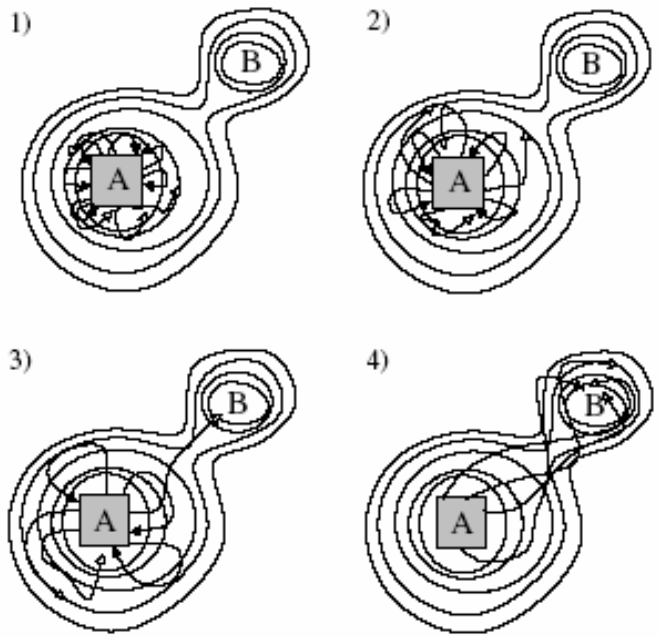

Fig. 5. Time as transition parameter. The square denotes the definition of the boundary for state A. The thin lines are free energy contour lines. The four panels show the representation of generated trajectories in successive time-interface ensembles. At panel (1), $\mathscr{P}_A(\mathscr{T}_{i+1}|\mathscr{T}_i)$ is the fraction of of trajectories that stay outside A longer than $\mathscr{T}_{i+1}$ (open arrows). All trajectories have at least a length $\mathscr{T}_i$. The solid arrows are the paths that return to A before $\mathscr{T}_{i+1}$. At panel (2), $\mathscr{P}_A(\mathscr{T}_{i+2}|\mathscr{T}_{i+1})$ is calculated for paths that remain outside A longer than $\mathscr{T}_{i+1}$. The minimum length of the paths is further increased at panel (3). Incidentally, a path will end up in the yet unknown state B. At panel (4) the minimum path length constraint forces all the paths into the metastable state region B. From here, they will not return. Hence, $\mathscr{P}_A(\mathscr{T}|0)$ will show a plateau.

T.S. van Erp, P.G. Bolhuis / Journal of Computational Physics 205 (2005) 157–181

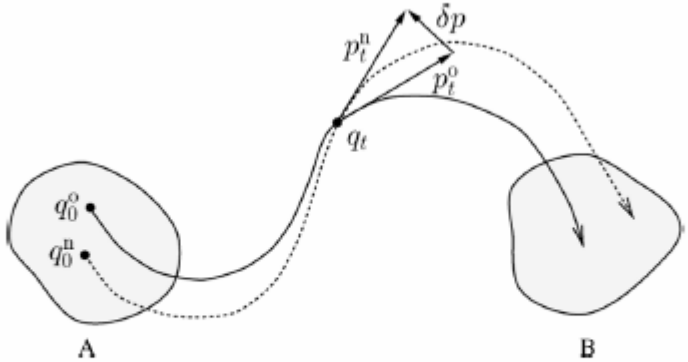

Fig. 1 Scheme of the shooting algorithm. A point r_t^o is selected at random along an existing path (——) connecting A with B. The momenta p_t^o at time t are then changed by a small amount δp creating the new momenta p_t^n. Starting from $\{q_t^o, p_t^n\}$ the new path (----) is calculated by forward and backward integration of the equations of motion. The new path is accepted according to a Metropolis criterion.

Faraday Discuss., 1998, 110, 421-436

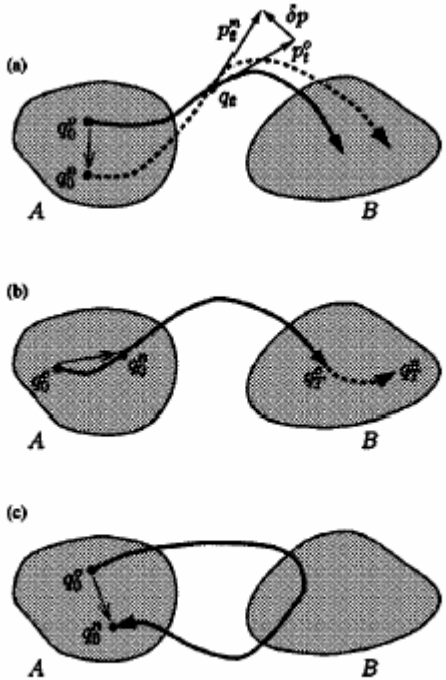

J. Chem. Phys., Vol. 110, No. 14, 8 April 1999

FIG. 1. Schematic representation of the shooting move (a), the shifting move (b), and the path reversal move (c).

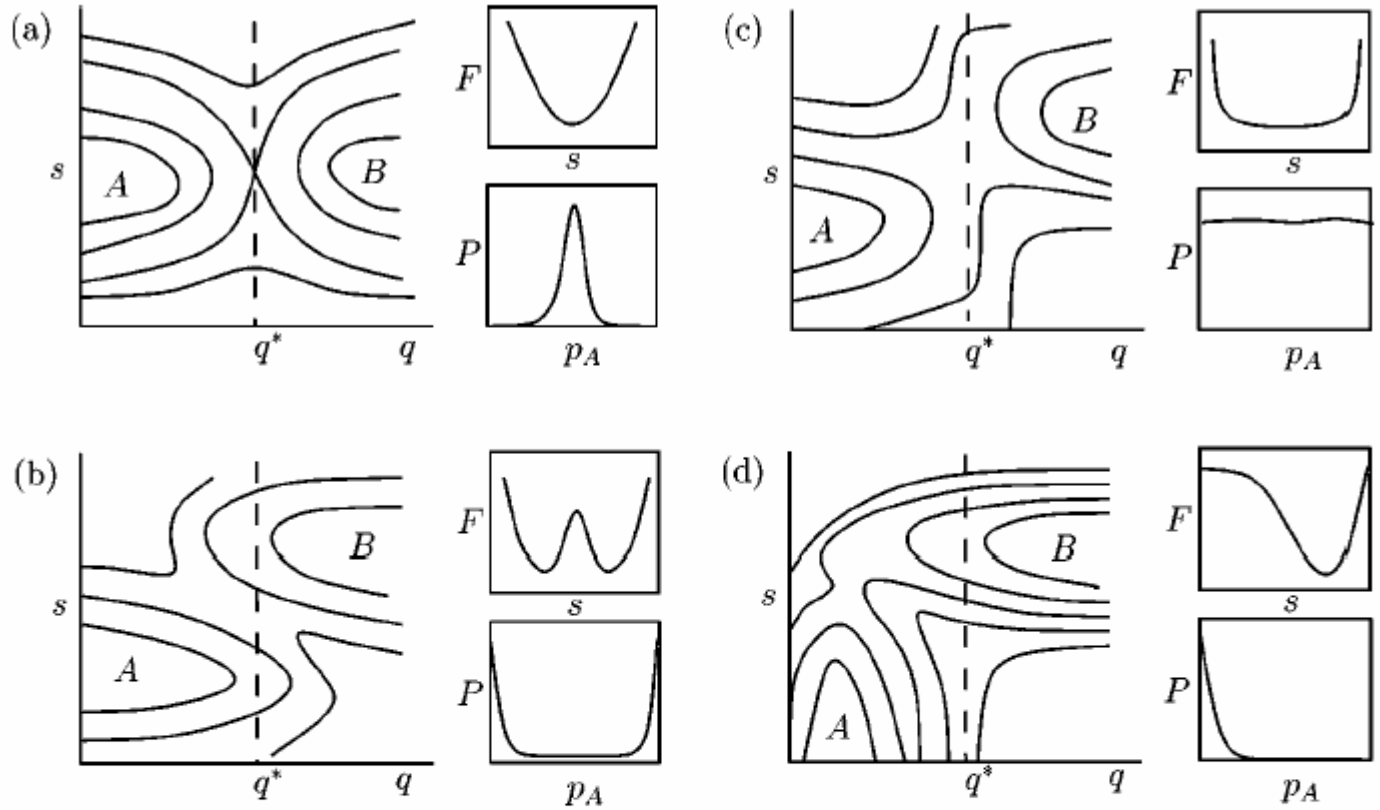

Figure 9 Four different potential or free-energy landscapes $V(q, s)$. Alongside each are plotted the corresponding free energy, $F(q^*, s)$, and committor distribution, $P(p_A)$, for the ensemble of microstates with $q = q^*$. For landscape (a), the reaction coordinate is adequately described by q, and $P(p_A)$ is peaked at $p_A = 1/2$. For landscape (b), the reaction coordinate has a significant component along s, as indicated by the barrier in $F(q^*, s)$ and the bimodal shape of $P(p_A)$. In (c), s is again an important dynamical variable. In this case $P(p_A)$ is nearly constant, suggesting that motion along s is diffusive when q is near q^*. Finally, for landscape (d), the reaction coordinate is orthogonal to q, reflected by the single peak of $P(p_A)$ near $p_A = 0$. In this case, almost none of the configurations belonging to the constrained ensemble with $q = q^*$ lie on the transition state surface.

Maier-Stein potential

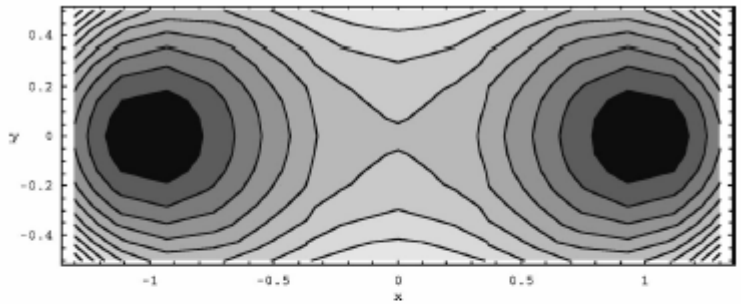

FIG. 1. The potential-energy surface of the Maier-Stein system, Eq. (3), with $\alpha=1$ and $\mu=1$. Darker shading indicates lower energies. Note the stable states at $(\pm 1,0)$, the transition state at $(0,0)$, and the surface dividing the stable states (the separatrix) at $x=0$. These general features persist for the other values of the parameters used in this paper, although the force field is no longer the gradient of a potential energy. For this equilibrium system the most probable path connecting the stable states (and therefore the path that dominates transitions in the weak noise limit) runs directly along the x axis.

networks [16]. As a particular example, we adopt the following two-dimensional system [$\mathbf{x}=(x,y)$] proposed by Maier and Stein [4], namely,

$$\mathbf{F}(x,y)=(x-x^3-\alpha xy^2,-\mu y(1+x^2)). \qquad (3)$$

This field is not the gradient of a potential energy unless $\alpha=\mu$. The potential-energy surface for the gradient field $\alpha=\mu=1$, is shown in Fig. 1, which should serve to orient the

Lennard-Jones clusters

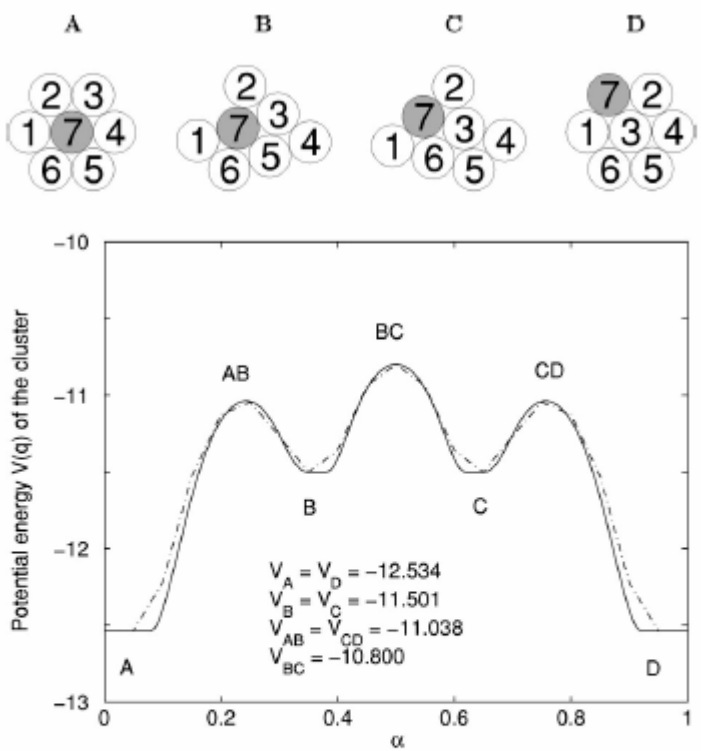

FIG. 1. Top figure: a transition pathway by which the central atom migrates to the surface in a seven-atom hexagonal Lennard-Jones cluster in the plane. The pictures show successive configurations corresponding to local minima of the potential energy along the path. Bottom figure: the potential energy along the path in natural units. The solid line corresponds to a simulation with $N=200$ discretization points along the string and the dashed line $N=20$.

PHYSICAL REVIEW B 66, 052301 2002

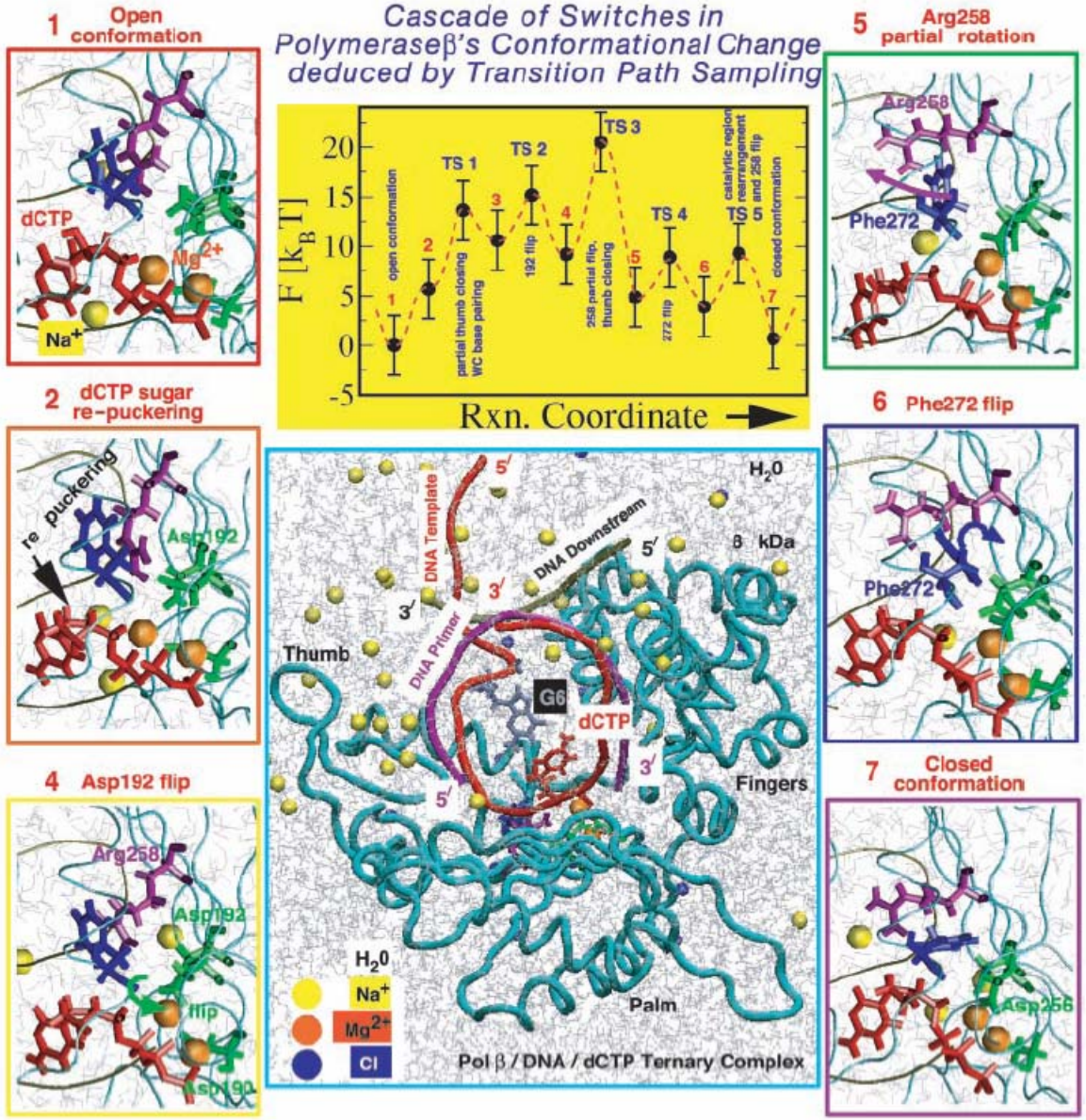

Fig. 4. (*Upper Center*) Overall captured reaction kinetics profile from TPS for pol β's closing transition (for a G·C system) from the open state and estimated energies in units of k_BT (product of Boltzmann constant and absolute temperature). Different barrier regions (TS) and metastable basins along the reaction coordinate are illustrated (images *1*, *2*, *4–6*, and *7*). (*Lower Center*) Structure of pol β/DNA/dCTP ternary complex.

Lasso/Bolas – Schlick et al.

- Harvest short trajectories
- 2-3 Simulations studies first
- Perl script implements TPS and calls CHARMM for all-atom dynamics

The shooting algorithm [6] generates an ensemble of molecular dynamics trajectories connecting two local minima (metastable states) A and B (see Fig. 8) in a free energy landscape via Monte Carlo sampling. For a given dynamics trajectory, the state of the system (i.e., basin A or B) is characterized by defining a set of order parameters $\chi = \{\chi_1, \chi_2, \cdots\}$. These order parameters are geometric quantities such as dihedral angles, bond distances, rms deviations of selected residues with respect to a reference structure, and so on. For biomolecules, as we show later, the key to a successful TPS application is identifying these key variables. Here, the groundwork simulations were important [7–9]. To formally identify a basin, *the population operator* h_A indicates if a particular molecular configuration associated with a time t of a molecular dynamics trajectory belongs to basin A:

J. Chem. Phys., Vol. 121, No. 5, 1 August 2004

In summary, we implement BOLAS for each χ_i defining a transition using the following steps.

(1) We define the order parameter window $\chi_{i,\min}<\chi_i<\chi_{i,\max}$ in which to calculate the free energy profile.

(2) We harvest dynamics trajectories according to the action in Eq. (3) but accept them only if they visit the window $\chi_{i,\min}<\chi_i<\chi_{i,\max}$ during time τ.

(3) We use the configurations contained within the ensemble of accepted trajectories to compute the probability distribution $P(\chi_i)$ according to Eq. (6) by constructing a histogram corresponding to χ_i.

(4) We combine the probability distributions $P(\chi)$ in successive windows by adjusting the constants in Eq. (8) to make $\Lambda_i(\chi_i)$ continuous.[21–23]

(5) We compute the relative free energies using Eq. (7).

$$H_B\{\chi\}^\tau = \begin{cases} 1 & \text{if there exists } 0<t<\tau \text{ such that } h_B(t)=1 \\ 0 & \text{otherwise} \end{cases}$$

Eq. 3 $$S\{\chi\}^\tau=\rho(0)h_A(\chi^0)H_B\{\chi\}^\tau,$$

$$P(\chi_i')\propto\int dr\,dp\,S\{\chi\}^\tau\sum_{j=1}^{\tau}\delta(\chi_i'-\chi_i^j), \tag{6}$$

$$\exp\{-\beta[F(B)-F(A)]\} = \int_{\chi_{i,B,\min}}^{\chi_{i,B,\max}} d\chi_i' P(\chi_i') \Big/ \int_{\chi_{i,A,\min}}^{\chi_{i,A,\max}} d\chi_i' P(\chi_i'), \tag{7}$$

$$\Lambda_i(\chi_i)=-k_BT\ln[P(\chi_i)]+\text{const.} \tag{8}$$

TPS Elaborated

biased sampling techniques [17–19]. Here, k_B is the Boltzmann constant and T is the temperature. The maximum λ^* in $F(\lambda)$ defines the dividing surface $\{x|\lambda(x) = \lambda^*\}$ separating state A from state B. By convention, the system is in A if $\lambda(x) < \lambda^*$ and in B if $\lambda(x) > \lambda^*$. For a phase point x in A, the probability to be at the top of the barrier is:

$$P(\lambda^*)_{x\in A} \equiv \frac{\langle \delta(\lambda(x) - \lambda^*)\rangle}{\langle \theta(\lambda^* - \lambda(x))\rangle} = \frac{e^{-\beta F(\lambda^*)}}{\int_{-\infty}^{\lambda^*} d\lambda\, e^{-\beta F(\lambda)}}, \tag{1}$$

where the brackets $\langle \cdots \rangle$ denote the equilibrium ensemble averages, $\theta(x)$ and $\delta(x)$ are the Heaviside step-function and the Dirac delta function, respectively, and $\beta = (k_B T)^{-1}$. TST assumes that trajectories that cross λ^* do not recross the dividing surface. Hence, the TST expression is equivalent to the positive flux through the dividing surface λ^*:

$$k_{AB}^{TST} = \left\langle \dot{\lambda}(x)\theta\left(\dot{\lambda}(x)\right)\right\rangle_{\lambda^*} P(\lambda^*)_{x\in A}, \tag{2}$$

where the dot denotes a time derivative and the subscript λ^* to the ensemble brackets indicates that the ensemble is constrained to the top of the barrier on the dividing surface λ^*. The TST rate constant is sensitive to the choice of reaction coordinate $\lambda(x)$ and will only be correct if the surface $\{x|\lambda(x) = \lambda^*\}$ corresponds to the true transition state dividing surface: the so-called separatrix at which no correlated recrossings occur. For complex systems, it is impossible to know the location and shape of this curved multidimensional separatrix and it is even questionable if such surface always exists. It is possible, however, to correct the TST expression with a dynamical factor that is called the transmission coefficient.

Journal of Computational Physics 205 (2005) 157–181

- *Main loop*
  (1) Take a uniform random number α_1 in the interval [0:1].
  (2) If $\alpha_1 < \gamma$ perform a time-reversal move. Otherwise, perform a shooting move.
  (3) If the trial path generated by either the time-reversal or shooting move is a proper path in the λ_i ensemble accept the move and replace the old path by the new one, otherwise keep the old path. Update averages and repeat from step 1.
- *Time-reversal move*
  (1) If the current path ends at λ_{i+1} reject the time-reversal move and return to the main loop.
  (2) If the current path starts and ends at λ_0, reverse the momenta and the order of time-slices. On this reverse path, x_0 is the new first crossing point with λ_i. Return to the main loop.
- *Shooting move*
  (1) On the current path with length $N^{(o)}$ choose a random time slice τ', with $-\tau^b \leqslant \tau' \leqslant \tau^f$.
  (2) Change all momenta of the particles at time-slice τ by adding small randomized displacements $\delta p = \delta w \sqrt{m}$ with δw taken from a Gaussian distribution with width σ_w and m the mass of the particle [14].
  (3) In case of constant temperature (NVT) simulations: accept the new momenta with a probability [4]:

$$\min\left[1, \exp\left(\beta\left(E(x^{(o)}_{\tau'\Delta t}) - E(x^{(n)}_{\tau'\Delta t})\right)\right)\right].$$

Here, $E(x)$ is the total energy of the system at phase space point x. In case of constant energy (NVE) simulations in which possibly also total linear or angular momentum should be conserved: rescale all the momenta of the system according to the procedure described in [37] and accept the new rescaled momenta.

If the new momenta are accepted continue with step 4, else reject the whole shooting move and return to the main loop.

(4) Take a uniform random number α_2 in the interval [0:1] and determine a maximum allowed path length for the trial move by:

$$N_{\max}^{(n)} = \mathrm{int}(N^{(o)}/\alpha_2).$$

(5) Integrate equations of motion backward in time by reversing the momenta at time slice τ', until reaching either λ_0, λ_{i+1} or exceeding the maximum path length $N_{\max}^{(n)}$. If the backward trajectory did not reach λ_0 reject and go back the main loop. Otherwise continue with step 6.

(6) Integrate from time slice τ' forward until reaching either λ_0, λ_{i+1} or exceeding the maximum path length $N_{\max}^{(n)}$. Reject and go back to the main loop if the maximum path length is exceeded or if the entire trial path has no crossing with interface λ_i. Otherwise continue with the next step.

(7) Accept the new path, reassign x_0 to be the first crossing point with λ_i and return to the main loop.

Finally, the probability $\mathscr{P}_A(\lambda_{i+1}|\lambda_i)$ follows from:

$$\mathscr{P}_A(\lambda_{i+1}|\lambda_i) = \frac{N_p(0 \to i+1)}{N_p(\mathrm{total})}, \tag{29}$$

with $N_p(0 \to i+1)$ the number of sampled paths that connect λ_0 with λ_{i+1} and $N_p(\mathrm{total})$ the total number sampled paths in the ensemble of interface λ_i.

Part II - Supersymmetric MD

New ‘MD’ equation

$$\frac{\partial W}{\partial t} = \left[-H_{\mathrm{K}} - \mathcal{N}(\mathbf{w}) + \sum_{i=1}^{2N} \frac{\partial}{\partial w_i} \left(\sum_{j=1}^{2N} A_{ij} w_j - \mathcal{N}(\mathbf{w}) w_i \right) \right] W,$$

$$\frac{\partial}{\partial t} W(\mathbf{q},\mathbf{p},t) = -H_{\mathrm{K}} W(\mathbf{q},\mathbf{p},t),$$

It has been shown [11,13] that a hidden supersymmetry is associated with the Kramers equation: By extending the space with $4N$-fermion operators

$$\{a_\mu, a_\nu^\dagger\} = \delta_{\mu\nu}, \quad \{b_\mu, b_\nu^\dagger\} = \delta_{\mu\nu}, \tag{8}$$

Supersymmetric version is

$$H_{\mathrm{SK}} = H_{\mathrm{K}} + \frac{1}{m} \sum_{\mu,\nu=1}^{N} \frac{\partial^2 V}{\partial q_\mu \partial q_\nu} b_\mu^\dagger a_\nu + \sum_{\mu=1}^{N} (\gamma b_\mu^\dagger b_\mu - a_\mu^\dagger b_\mu).$$

$$H_{\mathrm{K}} = \sum_{\mu=1}^{N} \left[\frac{\partial}{\partial q_\mu} \frac{p_\mu}{m} - \frac{\partial}{\partial p_\mu} \left(m\gamma T \frac{\partial}{\partial p_\mu} + \gamma p_\mu + \frac{\partial V}{\partial q_\mu} \right) \right].$$

Evolution eqn.

$$\frac{d}{dt} w_i = \mathcal{N}(\mathbf{w}) w_i - \sum_{j=1}^{2N} A_{ij} w_j.$$

$$\mathcal{N}(\mathbf{w}) = \frac{\mathbf{w}^{\mathrm{t}} A \mathbf{w}}{|\mathbf{w}|^2}.$$

$$A = \begin{pmatrix} 0 & -\delta_{\mu\nu}/m \\ \dfrac{\partial^2 V}{\partial q_\mu \partial q_\nu} & \gamma \delta_{\mu\nu} \end{pmatrix}.$$

PHYSICAL REVIEW E ***75****, 046707 2007*

“How does the presence of different time scales reflect in the one-fermion sector of the spectrum of *H*SK? In a simplified setting where entropy plays no role and the separation of time scales is purely due to the characteristics of the energy landscape, the use of a WKB technique in the limit $T \to 0$ shows explicitly 10 that, while the zero-fermion states are Gaussians centered on the local minima of the energy, the corresponding i.e., related by the supersymmetry onefermion states are the “reduced current” densities 11 obtained by applying the SuSy charge operator to the probability currents 7, concentrated on the saddles that separate those minima. In other words, the dynamics given by Eqs. 2 and 24 evolves in such a way that the walkers quickly that is, on a time scale larger than fast but much smaller than slow organize themselves into trails going from one local minimum to another one by overcoming the energy barrier along the reaction path 9.”

$$\dot{\mathbf{q}} = \mathbf{p}/m,$$

$$\dot{\mathbf{p}} = -\nabla V + \sqrt{2m\gamma T}\,\boldsymbol{\eta} - \gamma \mathbf{p}, \tag{2}$$

$$\frac{d}{dt} w_i = \mathcal{N}(\mathbf{w}) w_i - \sum_{j=1}^{2N} A_{ij} w_j. \tag{24}$$

In our implementation, the Langevin equation is solved by means of the second-order quasisymplectic integrator described in Ref. [29], while the conservation of the norm of the vector $\mathbf{w}$ is achieved by applying the implicit midpoint rule (see, for instance, Ref. [30]).

The friction coefficient entering the Langevin equation is set to $\gamma = 2.5\ \mathrm{ps}^{-1}$, and the mass of each particle is $m = 100$ amu. The time step used in all dynamical simulations is $\delta t = 10^{-4}$ ps. The SuSy MD simulations used $\sim 60\,000$ independent walkers for each temporal snapshot considered.

The simple tilted Mexican hat problem, and in general any two-dimensional situation, allows us also to understand the different roles played by partner eigenstates below the gap in the one and two fermion subspaces. As we have mentioned above, all the right two-fermion eigenstates which are partners to the loops can be obtained (always in two dimensions) from the zero-fermion left eigenstate of the inverted potential. This means that each corresponds to a constant in the region spanned by all trajectories descending from a saddle of index two (its unstable manifold), and this will be also true in more dimensions.

Langevin/Fokker-Planck processes can be immersed in a larger frame by adding fictitious fermion variables.

$$\frac{dR_c(x,t)}{dt} = -H_{FP}\, R_c(x,t) - \sum_{b=1}^{N} \frac{\partial^2 E}{\partial x_c \partial x_b} R_b(x,t). \qquad (7)$$

Equation (7) is one of the main instruments of this paper. It evolves a vector field $\boldsymbol{R}(x,t)$ so that it rapidly becomes a linear combination of one fermion states 'below the gap'.

In the low temperature limit there are two metastable states each concentrated around one of the minima. Barrier penetration leads to the Gibbs measure, the symmetric combination of those states. In fact the spectrum of the Fokker-Planck Hamiltonian will contain one zero eigenvalue $\lambda_0 = 0$ (the Gibbs measure), one small $\lambda_1 \sim O(e^{-\Delta/T})$ eigenvalue and the rest of them much larger ($O(1)$). The two pure states, localized on the right and on the left are $\propto \psi^{0R}(x) \pm \psi^{1R}(x)$, respectively. If we are interested in the dynamics of the passage between the two wells we have to consider times such that the fast relaxation within each well has already taken place. At such times, larger than $t_1 \sim \frac{1}{\lambda_2} log(\frac{c_2}{c_1})$, we are left only with a distribution

$$P(x, t \gg t_1) \simeq c_0 \psi^{0R} + c_1 \psi^{1R} e^{-\lambda_1 t}, \qquad (31)$$

i.e. a combination of states localized to the right and to the left, dependent upon the initial condition and time.

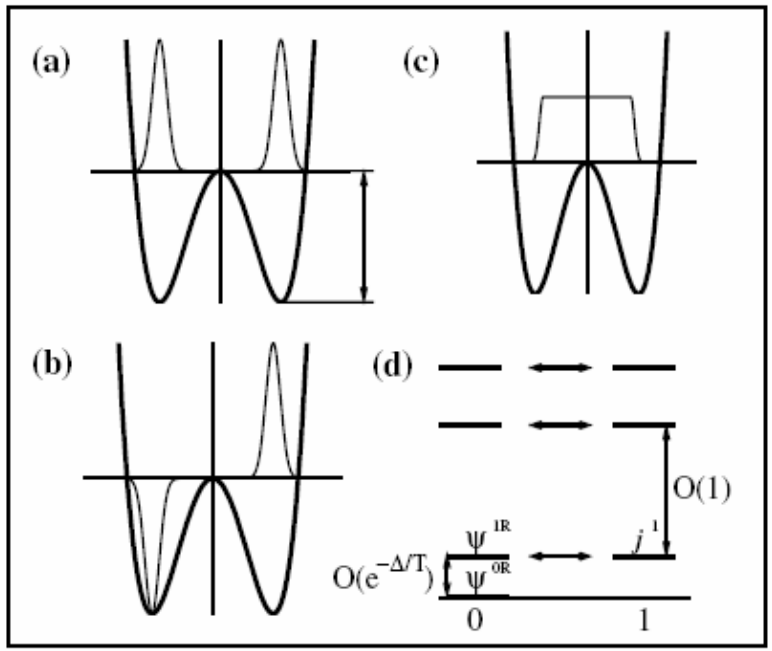

Fig. 3. The potential and different eigenstates along the reaction coordinate; (a) is the equilibrium density (ψ^{0R}), (b) the first eigenstate - the most stable (ψ^{1R}), (c) is the current density (j^1) from the first eigenstate and (d) the spectrum with the gap and the two fermionic sectors.

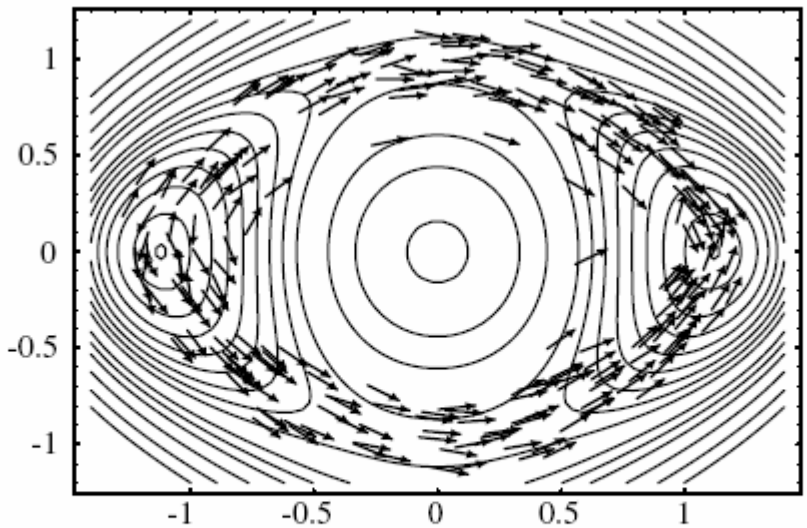

Fig. 7. Snapshot of a population of walkers in the stationary state. The potential is taken from.[37] It has two minima (right and left), two saddles (top and bottom) and a maximum in the center.

Work is in progress,[42,41] stimulated by the prejudice that things that are pleasant should also be useful.

Journal of Statistical Physics, Vol. 116, No. 5/6, September 2004

Mexican hat potential example, worked out:

A low temperature example will make things clearer. Consider the tilted Mexican hat in two dimensions (Fig. 4): it has a minimum, a maximum, and a 'blind' saddle, one that does not lead anywhere. The two-fermion lowest eigenstate is of the form

$$|\rho^R\rangle = a_x^\dagger a_y^\dagger |\rho^R\rangle \otimes |-\rangle, \tag{56}$$

where $\rho^R(x, y)$ satisfies:

$$-\left(T\frac{\partial}{\partial x} + \frac{\partial E}{\partial x}\right)\frac{\partial}{\partial x}\rho^R(x, y) - \left(T\frac{\partial}{\partial y} + \frac{\partial E}{\partial y}\right)\frac{\partial}{\partial y}\rho^R(x, y) = \lambda\rho^R(x, y), \tag{57}$$

which is easily obtained permuting (fermion) particles and holes in the Hamiltonian (13). The lowest-lying one-fermion eigenstate is obtained by noticing that the eigenvalue equation (57) corresponds to the equation satisfied by the *left* eigenstate of a Fokker-Planck equation in a the reversed potential $-E(x, y)$ (cfr. Eq. (20)). From the discussion in Section4, we conclude that ρ^R (the only $A(x, y)$ for the reversed problem) is essentially constant within the region spanned by all gradient lines descending from the local maximum (the unstable manifold of the maximum, or the stable manifold of the minimum of $-E$) – and drops sharply to zero at the border of this region. Acting with Q on ρ^R, we obtain the current:

$$\left(\chi_x^R(x, y), \chi_y^R(x, y)\right) \sim \left(\frac{\partial\rho^R}{\partial y}, -\frac{\partial\rho^R}{\partial x}\right), \tag{58}$$

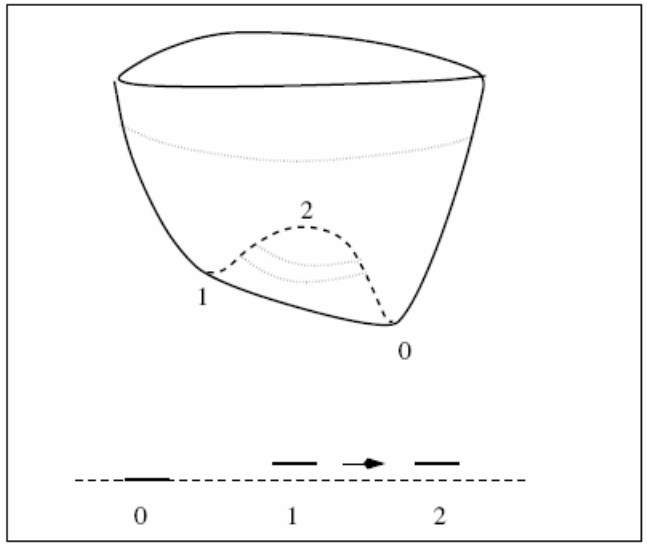

Fig. 4. A landscape with a minimum, a maximum and a blind saddle. Below: the low eigenvalue spectrum for zero, one and two fermions. The dotted line is the zero level, other eigenvalues are exponentially small in $1/T$. Next higher eigenvalues start at $O(1)$ (not shown).

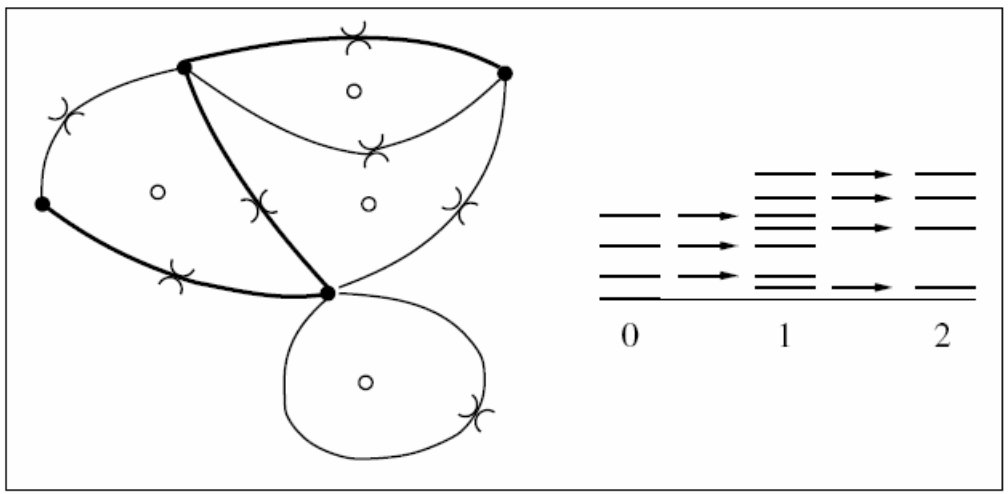

Fig. 5. A sketch of an energy surface with four minima (full circles), four maxima (open circles) and seven pathways passing through one saddles. The thick paths have a low activation times. On the right the corresponding spectrum of the Hamiltonian (13).

Ende

References:

Transition Path Sampling: Throwing Ropes Over Rough Mountain Passes, in the Dark
Peter G. Bolhuis, David Chandler, Christoph Dellago, and Phillip L. Geissler
Annu. Rev. Phys. Chem. 2002. 53:291–318

Sampling ensembles of deterministic transition pathways
Peter G. Bolhuis, Christoph Dellago and David Chandler
Faraday Discuss., 1998, 110, 421–436

Elaborating transition interface sampling methods
Titus S. van Erp and Peter G. Bolhuis
Journal of Computational Physics 205 (2005) 157–181

Efficient transition path sampling for nonequilibrium stochastic dynamics
Gavin E. Crooks and David Chandler
Physical Review E, Volume 64, 026109

On the calculation of reaction rate constants in the transition path ensemble
Christoph Dellago, Peter G. Bolhuis, and David Chandler
J. Chem. Phys., Vol. 110, No. 14, 8 April 1999

Illustration of transition path theory on a collection of simple examples
Philipp Metzner and Christof Schütte
Eric Vanden-Eijnden
J. Chem. Phys. 125, 084110 2006

Supersymmetric Langevin equation to explore free-energy landscapes
Alessandro Mossa and Cecilia Clementi
Physical Review E 75, 046707 2007

Introducing Supersymmetry
Martin F. Sohnius
Physics Reports 128, Nos. 2 & 3 (1985) 39–204

Kramers Equation and Supersymmetry
Julien Tailleur, Sorin Tanase-Nicola, and Jorge Kurchan
Journal of Statistical Physics, Vol. 122, No. 4, February 2006

Metastable States, Transitions, Basins and Borders at Finite Temperatures
Sorin Tanase-Nicola and Jorge Kurchan
Journal of Statistical Physics, Vol. 116, No. 5/6, September 2004

On the efficient sampling of pathways in the transition path ensemble
Thijs J. H. Vlugt and Berend Smit
PhysChemComm, 2001, 2, 1–7.